OCEAN CIRCULATION

A sea change in our view of overturning in the subpolar North Atlantic

M. S. Lozier[1]*, F. Li[1]*, S. Bacon[2], F. Bahr[3], A. S. Bower[3], S. A. Cunningham[4], M. F. de Jong[5], L. de Steur[5]†, B. deYoung[6], J. Fischer[7], S. F. Gary[4], B. J. W. Greenan[8], N. P. Holliday[2], A. Houk[9], L. Houpert[4], M. E. Inall[4,10], W. E. Johns[9], H. L. Johnson[11], C. Johnson[4], J. Karstensen[7], G. Koman[9], I. A. Le Bras[12], X. Lin[13], N. Mackay[14]‡, D. P. Marshall[15], H. Mercier[16], M. Oltmanns[7], R. S. Pickart[3], A. L. Ramsey[3], D. Rayner[2], F. Straneo[12], V. Thierry[17], D. J. Torres[3], R. G. Williams[18], C. Wilson[14], J. Yang[3], I. Yashayaev[8], J. Zhao[3]§

To provide an observational basis for the Intergovernmental Panel on Climate Change projections of a slowing Atlantic meridional overturning circulation (MOC) in the 21st century, the Overturning in the Subpolar North Atlantic Program (OSNAP) observing system was launched in the summer of 2014. The first 21-month record reveals a highly variable overturning circulation responsible for the majority of the heat and freshwater transport across the OSNAP line. In a departure from the prevailing view that changes in deep water formation in the Labrador Sea dominate MOC variability, these results suggest that the conversion of warm, salty, shallow Atlantic waters into colder, fresher, deep waters that move southward in the Irminger and Iceland basins is largely responsible for overturning and its variability in the subpolar basin.

Paleoceanographers have long interpreted millennial-scale climate variability in the context of ocean dynamics. Alternate periods of global cooling and warming have been attributed to variability in the Atlantic Ocean's meridional overturning circulation (MOC), brought about by changes in deep water production at high latitudes in the North Atlantic (*1*). A collection of studies in the 1990s (*2*) changed our perception of the time scale on which overturning variability could influence the climate. Synchronous changes recorded in ice sheets in Greenland and Antarctica revealed global atmospheric temperature disruptions on the scale of years to decades. In response to concerns about abrupt climate change raised by these studies, the United Kingdom and the United States deployed the RAPID Meridional Overturning Circulation and Heat-flux Array (RAPID-MOCHA) in 2004 at 26.5°N in the subtropical North Atlantic to provide the first continuous direct measure of the overturning (*3*). Data from this array revealed strong variability on all observed times scales, substantially altering our view of the overturning circulation (*4*).

In the 14 years since the RAPID-MOCHA array was deployed, modeling and observational studies have suggested that overturning variability is not coherent between the subtropical and subpolar latitudes on interannual to decadal scales (*5*–*7*). Furthermore, modeling studies have shown that interannual variability in the RAPID-MOCHA time series can be largely reproduced by wind forcing alone (*8*) and that wind variability may also be important in forcing overturning variability at 26.5°N on decadal time scales (*9*). These studies, along with other modeling results, which suggest that buoyancy-forced MOC changes have larger amplitude in the subpolar North Atlantic (SPNA) (*10*), led to strong interest in a complementary measure of the overturning circulation in this region, where the link between deep water mass formation and overturning variability could be directly assessed. Underscoring the importance of this assessment, the most recent Intergovernmental Panel on Climate Change report projects a MOC slowdown in the 21st century and attributes that slowdown to a reduction in deep convection in the North Atlantic (*11*). Furthermore, evidence continues to mount that sustained observations of the MOC are needed to understand the potential impact of overturning variability on anthropogenic carbon uptake and storage in the North Atlantic (*12*).

OSNAP observing system

With contributions from the United States, the United Kingdom, Germany, the Netherlands, Canada, and China, the OSNAP observing system (Fig. 1) (*13*) comprises an integrated coast-to-coast array of two sections: OSNAP West, extending from the southeastern Labrador shelf to the southwestern tip of Greenland, and OSNAP East, extending from the southeastern tip of Greenland to the Scottish shelf. Densely spaced OSNAP mooring arrays, which directly measure the temperature, salinity, and velocity fields, are in place at continental boundaries and on both flanks of the Reykjanes Ridge; additional dynamic height moorings at key locations allow us to estimate geostrophic flows (Fig. 2). Glider surveys along topographically complex sections of OSNAP East complement the moored arrays. The observing system also includes subsurface acoustically tracked floats that trace the pathways of overflow waters in the basin. We report here the MOC, MHT (meridional heat transport), and MFT (meridional freshwater transport) time series from the full installation of the arrays in August 2014 until the first complete data recovery in April 2016. In addition to the OSNAP data, our MOC, MHT, and MFT estimates rely on Argo profiling float data, satellite altimetry, and surface wind fields (*14*).

The deployment of the OSNAP array in the summer of 2014 was auspiciously timed; the following two winters produced strong cooling in the western SPNA, with clear signatures of newly formed water in the Irminger Sea (*15*–*17*) and mixed-layer depths in the range of 1500 to 2000 m in the Labrador Sea (*16*, *18*). Convection to these depths has not occurred since the mid-1990s, when record deep water mass formation took place. Large pools of low-salinity waters in these basins (Fig. 2) are a strong signature of the recent convection.

MOC definition

We define the MOC as the maximum of the overturning stream function [in sverdrups (Sv), where 1 Sv = 10^6 m^3 s^{-1}] in density space (see supplementary materials). We choose density coordinates for our calculation because we are interested in the total volume of buoyant water moving northward (the upper limb) that is balanced by denser, deeper waters moving southward (the lower limb) across the OSNAP section. Here, the MOC upper (or lower) limb is defined as the transport between the sea surface (or bottom) and the density surface at which the overturning stream function reaches a maximum. Essentially, the MOC in density space measures the transformation of less-dense waters to more-dense waters that occurs poleward of the OSNAP line. This choice is particularly apt for the subpolar basin, where strongly sloped isopycnals (Fig. 2) confound the interpretation of the MOC calculated in depth space (*19*, *20*). By way of illustration, an integration of the flow across

[1]Division of Earth and Ocean Sciences, Duke University, Durham, NC, USA. [2]National Oceanography Centre, Southampton, UK. [3]Woods Hole Oceanographic Institution, Woods Hole, MA, USA. [4]Scottish Association for Marine Science, Oban, UK. [5]Royal Netherlands Institute for Sea Research and Utrecht University, Texel, Netherlands. [6]Department of Physics and Physical Oceanography, Memorial University, St. John's, Newfoundland, Canada. [7]GEOMAR Helmholtz Centre for Ocean Research Kiel, Kiel, Germany. [8]Bedford Institute of Oceanography, Dartmouth, Nova Scotia, Canada. [9]Department of Ocean Sciences, University of Miami, Miami, FL, USA. [10]School of Geosciences, University of Edinburgh, Edinburgh, UK. [11]Department of Earth Sciences, University of Oxford, Oxford, UK. [12]Scripps Institution of Oceanography, UCSD, La Jolla, CA, USA. [13]Physical Oceanography Laboratory and Institute for Advanced Ocean Studies, Ocean University of China and Qingdao National Laboratory for Marine Science and Technology, Qingdao, China. [14]National Oceanography Centre, Liverpool, UK. [15]Department of Physics, Oxford University, Oxford, UK. [16]CNRS, Laboratoire d'Océanographie Physique et Spatiale, Plouzané, France. [17]IFREMER, Laboratoire d'Océanographie Physique et Spatiale, Plouzané, France. [18]Department of Earth, Ocean and Ecological Sciences, University of Liverpool, Liverpool, UK.
***Corresponding author. Email: mslozier@duke.edu (M.S.L.); feili.li@duke.edu (F.L.)** †Present address: Norwegian Polar Institute, Tromsø, Norway. ‡Present address: Department of Geography, University of Exeter, Devon, UK. §Present address: University of Maryland Center for Environmental Science, Cambridge, MD, USA.

~500 m would include the warm, relatively buoyant northward-flowing waters in the eastern part of the basin and the cold, relatively dense southward-flowing waters off the east coast of Greenland, leading to an underestimate of the amount of water transformed, or "overturned," from one density class to another (table S2).

We refer to our MOC measure as the "overturning" and make no assumptions about its driving mechanisms, i.e., the overturning can be affected by buoyancy and/or wind forcing. We use Monte Carlo simulations to estimate the mean MOC, as well as the mean MHT and MFT, and to provide an estimate of the uncertainty in those means (see supplementary materials). All reported deviations (±) from the mean are uncertainty estimates, unless indicated otherwise. Finally, we note that the MOC definition reduces the complexity of the circulation across the OSNAP line to a two-layer system, a simplification that is robust for OSNAP East, yet less so for OSNAP West because of a number of opposing flows in that basin (fig. S1B).

Elements of the overturning and gyre circulation in the SPNA

A view of salinity and the west-to-east cumulative volume transport for the upper and lower limbs across the OSNAP line reveals the key elements of both the overturning and gyre circulation in the SPNA (Fig. 2). Across the Labrador Basin, the large pool of low-salinity water that reaches from the surface to ~1500 m marks the Labrador Sea Water (LSW), the shallowest component of the MOC lower limb. Some of this water mass is exported to the subtropics and some recirculates within the subpolar basin, the latter revealed by the pool of relatively fresh water at intermediate depths (1000 to 2000 m) in the Iceland Basin. A mixture of LSW and locally formed intermediate water is also visible in the Irminger Sea (500 to 1500 m). The western and

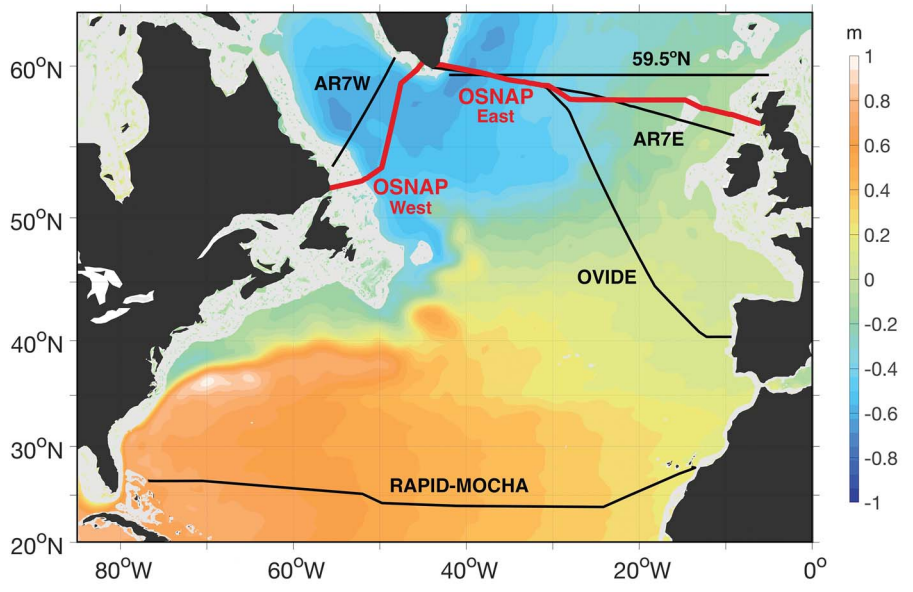

Fig. 1. OSNAP observing system. The OSNAP section (red line) superposed on a map of mean absolute dynamic height (meters), with bathymetry <500 m shaded gray. The OSNAP observing system was designed to take advantage of the German Labrador Sea exit array at 53°N (operational since 1997) (*32*); the recently installed U.S. Global OOI (Ocean Observatories Initiative) node in the southwest Irminger Sea; repeat A1E/AR7E hydrographic sections across the Irminger and Iceland basins (*42*, *43*); and the Ellett Line in the eastern basin (operational since 1976) (*44*). OSNAP complements several monitoring programs in the North Atlantic: the Canadian repeat AR7W program in the Labrador Sea (*18*, *45*), Cape Farewell-Scotland sections at 59.5°N (*29*, *30*), the French OVIDE line across the eastern North Atlantic (*22*), and the U.K.-U.S. RAPID-MOCHA array at 26.5°N (*3*).

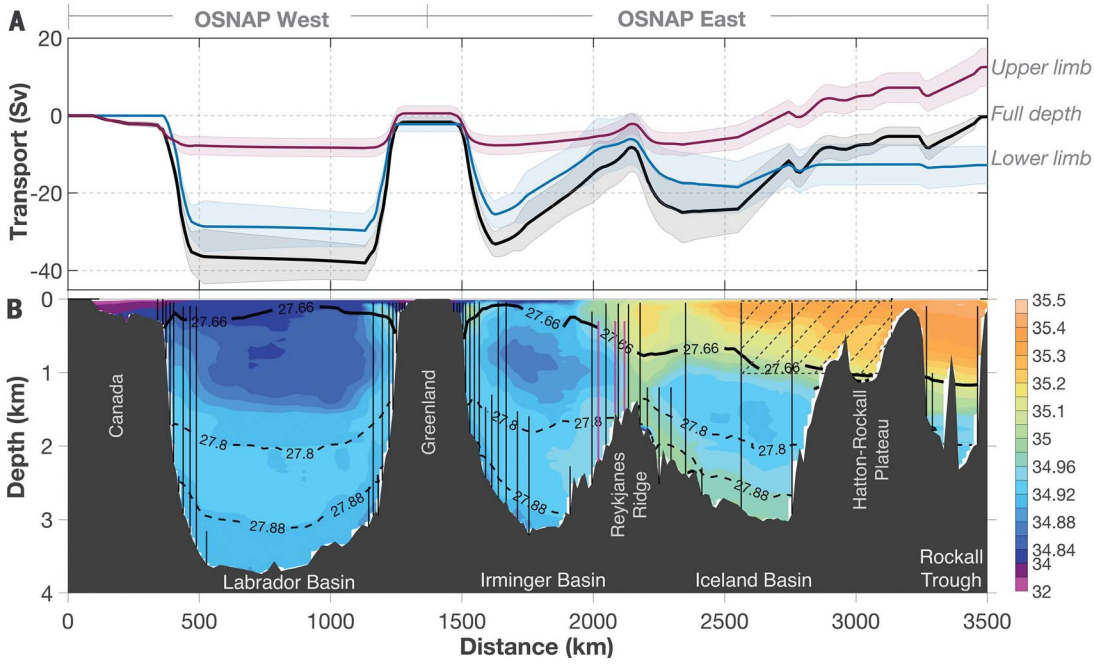

Fig. 2. Transport and salinity across the OSNAP section. (**A**) Top-to-bottom integrated volume transport accumulated eastward starting at the western edge of the Labrador Basin (black line), with northward transport defined as positive. The upper (red line) and lower (blue line) MOC limbs are shown separately. Shading indicates one standard deviation from the 21-month mean. (**B**) The OSNAP section with moorings marked by vertical black lines. Vertical magenta lines on the western flank of the Reykjanes Ridge indicate three French moorings, which are part of the RREX program. Hatching in the eastern Iceland Basin indicates the glider survey domain. Mean salinity (colored, with scale at the right-hand side) and potential density (contoured) are calculated from Argo and OSNAP data from August 2014 to April 2016. The thick black line denotes the potential density surface (27.66 kg m^{-3}) that separates the MOC upper and lower limbs (see fig. S1A).

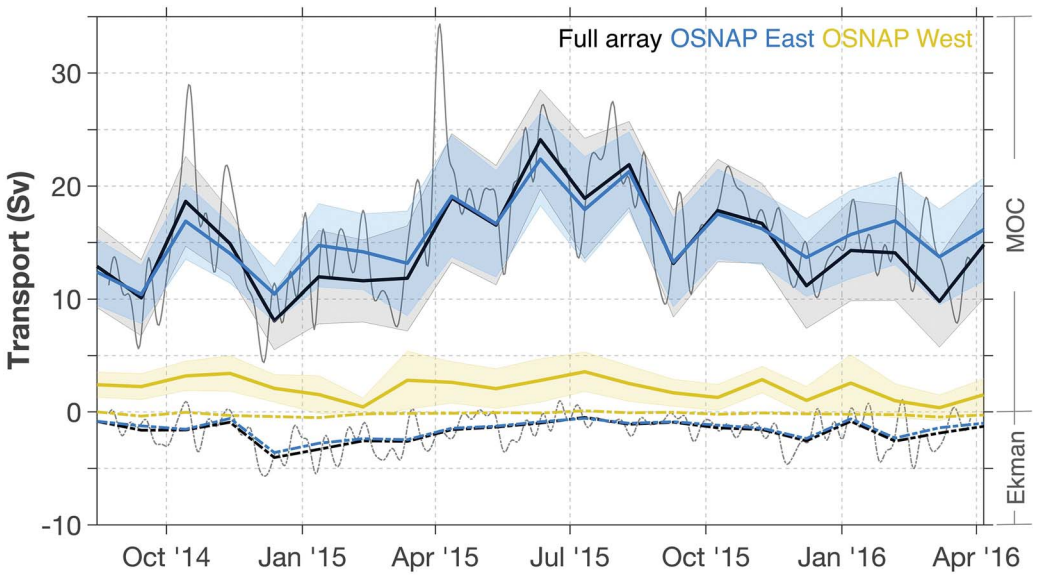

Fig. 3. MOC and Ekman transport across the OSNAP section. Black, yellow, and blue lines represent the 30-day mean estimates from the full section, OSNAP West, and OSNAP East, respectively, for MOC (solid lines) and Ekman transport (dashed lines). Shading indicates uncertainty in the 30-day means. Uncertainty in the Ekman transports is too small for display (see table S3). Thin gray lines show the 10-day low-pass filtered daily means for the full OSNAP section. See supplementary materials for details on the mean and uncertainty estimates.

eastern boundary currents in the Labrador Basin have strong transports, particularly so for the lower limb where transports reach ~30 Sv. However, the relatively small cumulative transport across the Labrador Sea in both the upper and lower limbs reveals that these opposing boundary currents are largely carrying waters of the same density, i.e., there is little density transformation or overturning across this basin during this time period.

Across OSNAP East, strong boundary currents with broader opposing flows in the basin interior are also evident in the lower limb (Fig. 2). Here, however, there is an appreciable accumulation of southward flow (~12 Sv), helped in part by the entry of cold overflow waters from the Nordic Seas into the subpolar basin. The relatively salty Iceland Scotland Overflow Water flows southward along the eastern flank of the Reykjanes Ridge, and the fresher Denmark Strait Overflow Water flows southward in the deep boundary current off East Greenland. The net southward transport of these deep components of the lower limb is largely balanced by the northward-flowing North Atlantic Current, which carries warm, salty waters across the easternmost part of the OSNAP section, forming the bulk of the upper MOC limb.

OSNAP MOC time series

Over the 21-month observational period, the MOC across the entire OSNAP section shows considerable temporal variability (Fig. 3), with 30-day means from 8.1 to 24.1 Sv, a range comparable to that observed at the RAPID-MOCHA array (*21*) and the OVIDE section (*22*). Not surprisingly, the daily means show a larger range, likely a result of high-frequency wind variability over the basin. Though we note a MOC peak in the summer of 2015, no evidence of seasonality can be gleaned from this short record. The net southward Ekman transport (−1.72 ± 0.02 Sv), resulting from the predominantly westerly winds across the OSNAP line, contributes only minimally to the time-mean and time-varying MOC (Fig. 3).

These time series highlight the most notable aspect of this 21-month record, namely that the overturning circulation across OSNAP East (15.6 ± 0.8 Sv) dominates that across OSNAP West (2.1 ± 0.3 Sv), the former being ~7 times greater than the latter. The sum of the MOC estimates across these two sections exceeds the MOC across the entire section (14.9 ± 0.9 Sv) because of cancellations between northward and southward transports. Specifically, southward currents along the east Greenland coast that round Cape Farewell cancel some of the northward flow in the same density class along the west Greenland coast, thus making the MOC estimate across the entire section less than the sum of its parts (fig. S1). The OSNAP East MOC estimate and the MOC estimate across the entire section are not distinguishable given our measure of uncertainty.

The overturning circulation across OSNAP East also dominates in terms of temporal variability. Overturning variability across this section explains 88% of the variance in the MOC across the entire section, far exceeding the contribution of OSNAP West (25%). The MOC time series across the two separate sections are only weakly correlated [at zero lag, the correlation coefficient (r) = 0.25; the correlation is strongest (r = −0.34) when MOC at OSNAP East leads by 4 months]. A longer time series will aid our understanding of the relationship between these two time series.

The contrast between the small overturning measure for OSNAP West and the signature of strong local convection (i.e., the homogeneous water mass) in this basin is sharp but not altogether surprising. A number of studies over the past decade have suggested that boundary current strength, exchange between the boundary and the basin interior, and/or other physics allow for a disconnect between local water mass production and its export out of the basin (*23*–*25*). These early OSNAP results provide support for that disconnect.

Comparison with other MOC estimates

A comparison of basin-wide MOC estimates in the North Atlantic is now possible with the OSNAP and RAPID-MOCHA arrays (table S3). Over a comparable time period, the OSNAP MOC mean is weaker by ~2 Sv than the MOC at 26.5°N (16.8 Sv for 2014–2016) (*21*). Although this RAPID-MOCHA MOC estimate is calculated in depth space, a measure in density space has been shown to be nearly identical owing to the relatively flat isopycnals across the subtropical gyre (*19*). A difference of 2 Sv is not large in light of the ~1 Sv uncertainty in the estimates of both the OSNAP and RAPID-MOCHA means (*26*). Insight into whether the subpolar MOC is actually weaker than the subtropical MOC will likely only be ascertained once a longer OSNAP time series is secured. Finally, the OSNAP estimate falls near the midpoint of the large range of SPNA MOC estimates predicted by a suite of global ocean-sea-ice models (~5 to 25 Sv) (*27*). The OSNAP observations will help narrow the range of these model estimates by providing useful benchmarks and validations.

Comparisons of the MOC across OSNAP East and West with the MOC from geographically similar locations are generally favorable. The OSNAP West estimate is consistent with the mean derived using Argo floats in the vicinity of the AR7W line from 2002 to 2016 (2.5 Sv) (*28*) and is also consistent with the mean estimated from summer hydrography and PALACE (Profiling Autonomous Lagrangian Circulation Explorer) floats (2 Sv) (*25*) in the same region between 1990 and 1997. There are two MOC estimates at 59.5°N, just north of the OSNAP East line: one is a 2002–2008 mean summer estimate (16.6 ± 1.1 Sv) (*29*) based on altimetry and hydrography, and the other is a long-term mean estimate from early 2012 to early 2016 based on hydrography and shipboard ADCP (Acoustic Doppler Current Profiler) measurements

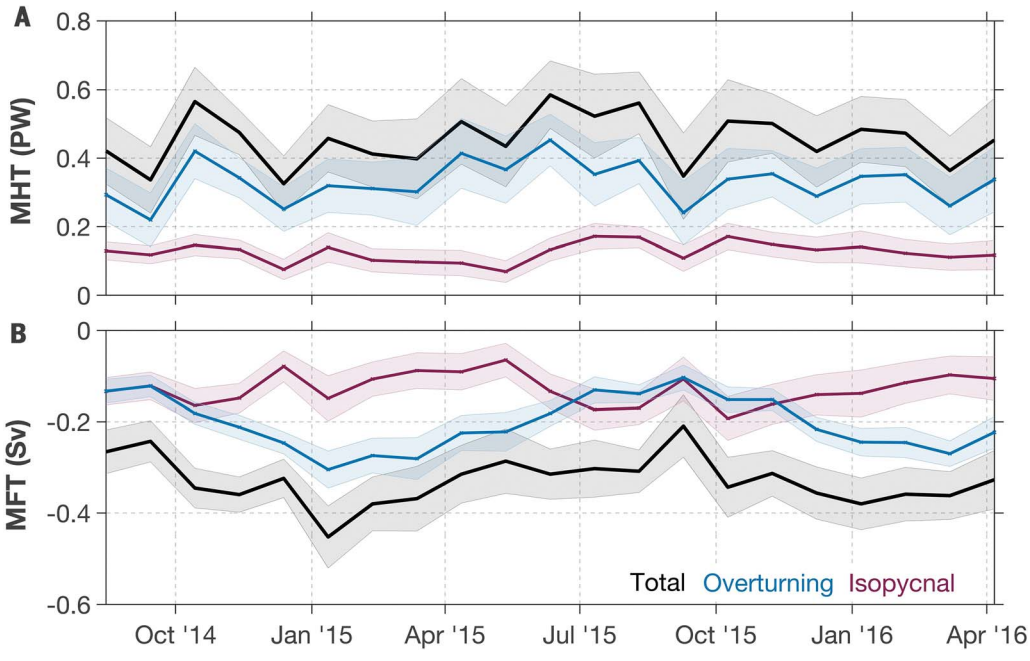

Fig. 4. MHT and MFT across the OSNAP section. (**A**) Total MHT. (**B**) Total MFT relative to the 21-month section mean salinity of 34.92 across the full OSNAP section during the period of August 2014 to April 2016 (black lines). Both transports are decomposed into overturning and isopycnal components (blue and red lines, respectively). Shading indicates uncertainty in the 30-day mean estimates. See supplementary materials for details on the mean and uncertainty estimates, as well as the decomposition.

(18.4 ± 3.4 Sv) (*30*). Given the uncertainties in all estimates, the OSNAP East MOC is largely consistent with these measures despite the fact that the records are noncontemporaneous. Finally, the OSNAP East estimate is somewhat lower than the MOC estimate, reconstructed from altimetry and Argo data, along the OVIDE line (which runs from Greenland to Portugal) (Fig. 1) between 1993 and 2010 (18.1 ± 1.4 Sv) (*22*). This difference is perhaps attributable to the presence of a subtropical component in the total OVIDE overturning, though further analysis is needed to confirm this supposition.

Meridional heat and freshwater transports

An estimate of MHT across the entire OSNAP section yields a mean and uncertainty of 0.45 ± 0.02 PW. The record is marked by strong temporal variability (Fig. 4), with a range of 0.33 to 0.59 PW. This variability is largely determined by the variable flow field rather than by temperature fluctuations: velocity variance explains 93% of the MHT variance. To understand the circulation features responsible for this heat transport, we decompose the total transport into an overturning component and an isopycnal transport component (see supplementary materials). In other words, we partition the heat transport into the following: (i) that which is accomplished by warm water moving northward in the upper limb and cold water moving southward in the lower limb (the overturning component) and (ii) that which is accomplished by opposing northward and southward flows (i.e., carrying waters with different temperatures) on the same isopycnal (the isopycnal transport component). This decomposition reveals that the overturning component dominates the total MHT (Fig. 4), accounting for 73% of the mean and 87% of the variance. Given this dominance, it is not surprising that the heat transport across OSNAP East (0.38 ± 0.02 PW) greatly exceeds that of OSNAP West (0.080 ± 0.004 PW) (table S3). A decomposition of heat transport in depth space (fig. S2) yields a relatively minor contribution of the overturning component to the total, illustrating the suitability of density coordinates for an estimate of how water mass transformation affects heat transport in the subpolar region.

The mean MFT across the entire OSNAP section is estimated at −0.33 ± 0.01 Sv. The MFT time series also reveals strong temporal variability (Fig. 4), with a range of −0.45 to −0.21 Sv. As with MHT, the majority of the MFT variance is explained by the variable flow field: velocity variability (rather than salinity variability) explains 78% of the total MFT variance. From the decomposition, we find that, on average, overturning accounts for 62% of the total freshwater transport across the full OSNAP array. However, there is considerable range in that partitioning, and there is a period of time (July to November of 2015) when the isopycnal component is larger. During this time period, the net southward flux of fresh water due to opposing flows on isopycnals is larger than the net southward freshwater flux accomplished by the overturning. Additionally, the contribution from OSNAP West (−0.184 ± 0.004 Sv) to the total MFT actually exceeds that from OSNAP East (−0.14 ± 0.01 Sv) (table S3), in contrast to their relative contributions to MHT. Note that we currently use monthly mean model velocities and monthly climatological means for salinity and temperature across the Labrador Current inshore of 300 m (see supplementary materials), where moored instrumentation is subject to disruption due to heavy fishing activity in the region. An exploration of alternative means for estimating the inshore velocity and properties is under way.

In summary, heat transport across the entire OSNAP section is principally accomplished by the overturning, which is largely focused across OSNAP East. In contrast, freshwater transport across OSNAP West is larger than that across OSNAP East, and the isopycnal component can at times exceed the overturning component. These differences can be understood in the context of circulation differences across OSNAP East and West (Fig. 2). The upper limb of OSNAP East has an isopycnal circulation (the volume of water with opposing northward and southward flows) of ~13 Sv, which nearly matches the transport of the overturning circulation (~15 Sv). However, the upper limb of OSNAP West has a much stronger isopycnal circulation (~11 Sv) than overturning circulation (~2 Sv). Thus, it appears that salinity gradients on isopycnals across OSNAP West may be driving a sizeable portion of the freshwater flux, a supposition that will be explored in future work by partitioning the MHT and MFT components across both OSNAP East and West. Such partitioning may help to reconcile our results with those of an earlier study (*25*), which found that isopycnal transport, rather than overturning, was the largest contributor to heat flux across the Labrador Sea during the 1990s.

Comparison with the RAPID-MOCHA MHT and MFT estimates

The simultaneous measure of MHT and MFT across the transatlantic OSNAP and RAPID-MOCHA lines provides, for the first time, an in situ measure of the heat and freshwater flux divergence between the two latitudes, quantities relevant to our understanding of climate variability and MOC stability. The heat transport divergence between these two lines, 0.80 PW (table S3), is the amount of heat stored or lost to the atmosphere as the warm Gulf Stream and North Atlantic Current waters

move northward from RAPID-MOCHA to OSNAP. Likewise, the southward OSNAP MFT is 0.10 Sv weaker than that reported at RAPID-MOCHA, suggesting a net freshwater storage or addition to the Atlantic between the two latitudes. These divergences provide an important validation for atmospheric reanalyses and air-sea flux estimates, which currently underestimate the northward ocean heat transport at the OSNAP latitudes (*31*).

Implications

These OSNAP results show that the conversion of warm, salty, shallow Atlantic waters into cold, fresh, deep waters that is accomplished north of the OSNAP East line is largely responsible for overturning and its variability in the subpolar basin over the course of this observational record. Despite signatures of substantial water mass formation, the Labrador Sea contributes minimally to the total overturning. This result is consistent with a number of recent studies that have raised questions about the importance of LSW formation to MOC variability. An examination of transports at 53°N (the westernmost array in the OSNAP West line) shows no clear link between boundary current export and LSW formation in the basin interior (*32*); a modeling study (*33*) finds no relationship between the volume of LSW formed in the Labrador Sea and its export to the subtropical gyre; and even further downstream, at the RAPID-MOCHA array, LSW variability is relatively weak and plays almost no role in the recent overturning decline (*21*).

Past modeling studies, however, have shown that density anomalies in the Labrador Sea are strongly associated with downstream MOC variability on multiannual to decadal time scales (e.g., *34*–*37*). Even though these time scales exceed the OSNAP observational record to date, the OSNAP MOC estimate stands in stark contrast to a picture of the MOC dominated by Labrador Sea convection. Furthermore, recent studies have used densities at mid-depth in the Labrador Sea, which are assumed to be linked to convection in that basin, as proxies for the modern and paleo Atlantic MOC (*38*–*40*). A reconciliation with these past modeling results is possible if the density anomalies in the Labrador Sea are signatures of upstream density anomalies imported from the eastern subpolar gyre and/or have a remote impact on the overturning between Greenland and Scotland. With either scenario, Labrador Sea density remains a signature of the MOC across the subpolar basin, yet not of local convection. In light of these new observations, further modeling studies are warranted, as is continued work on the use and interpretation of proxies (*41*).

Although these OSNAP observations invite a reexamination of some long-held assumptions about the MOC in the SPNA, a longer time series will be needed to determine whether the strong MOC across OSNAP East is consistent with buoyancy forcing north of the line and whether the relatively small overturning across OSNAP West reported here is representative of its contribution on longer time scales. Finally, whereas the MOC and MHT are dominated by OSNAP East dynamics, OSNAP West dynamics play a large role in the total MFT.

Next steps

An extension of this record is necessary to determine seasonal and interannual variability and to detect any long-term trends. However, it is of sufficient length to provide a baseline for numerical models, which is essential to placing the observations in a broader spatial and temporal context. Another important next step for the ocean community is to place these OSNAP results in the context of other Atlantic MOC measures to understand how overturning affects the basin-wide transport and storage of heat, fresh water, and carbon. A continuation of measurements is needed to achieve this objective, but the observing systems put in place during the past 15 years by the international ocean community are already yielding rich dividends and leading us in that direction.

REFERENCES AND NOTES

1. W. S. Broecker, *The Glacial World According to Wally* (Eldigio Press, ed. 2, 1995).
2. National Research Council, *Abrupt Climate Change: Inevitable Surprises* (National Academies Press, 2002).
3. S. A. Cunningham *et al.*, *Science* **317**, 935–938 (2007).
4. M. A. Srokosz, H. L. Bryden, *Science* **348**, 1255575 (2015).
5. R. J. Bingham, C. W. Hughes, V. Roussenov, R. G. Williams, *Geophys. Res. Lett.* **34**, L23606 (2007).
6. M. S. Lozier, V. Roussenov, M. S. C. Reed, R. G. Williams, *Nat. Geosci.* **3**, 728–734 (2010).
7. R. G. Williams, V. Roussenov, D. Smith, M. S. Lozier, *J. Clim.* **27**, 698–719 (2014).
8. J. Zhao, W. Johns, *J. Geophys. Res. Oceans* **119**, 2403–2419 (2014).
9. I. Polo, J. Robson, R. Sutton, M. A. Balmaseda, *J. Phys. Oceanogr.* **44**, 2387–2408 (2014).
10. A. Biastoch, C. W. Böning, J. Getzlaff, J.-M. Molines, G. Madec, *J. Clim.* **21**, 6599–6615 (2008).
11. IPCC, *Climate Change 2013: The Physical Science Basis*, T. F. Stocker, D. Qin, G.-K. Plattner, M. Tignor, S. K. Allen, J. Boschung, A. Nauels, Y. Xia, V. Bex, P. M. Midgley, Eds. (Cambridge Univ. Press, 2013).
12. G. A. McKinley, A. R. Fay, N. S. Lovenduski, D. J. Pilcher, *Annu. Rev. Mar. Sci.* **9**, 125–150 (2017).
13. M. Susan Lozier *et al.*, *Bull. Am. Meteorol. Soc.* **98**, 737–752 (2017).
14. F. Li, M. S. Lozier, W. E. Johns, *J. Atmos. Ocean. Technol.* **34**, 1483–1500 (2017).
15. M. F. de Jong, L. de Steur, *Geophys. Res. Lett.* **43**, 7106–7113 (2016).
16. A. Piron, V. Thierry, H. Mercier, G. Caniaux, *Geophys. Res. Lett.* **44**, 1439–1447 (2017).
17. F. Fröb *et al.*, *Nat. Commun.* **7**, 13244 (2016).
18. I. Yashayaev, J. W. Loder, *Geophys. Res. Lett.* **44**, 1429–1438 (2017).
19. X. Xu, E. P. Chassignet, W. E. Johns, W. J. Schmitz Jr., E. J. Metzger, *J. Geophys. Res. Oceans* **119**, 5140–5159 (2014).
20. N. P. Holliday *et al.*, *J. Geophys. Res. Oceans* **123**, 4538–4559 (2018).
21. D. A. Smeed *et al.*, *Geophys. Res. Lett.* **45**, 1527–1533 (2018).
22. H. Mercier *et al.*, *Prog. Oceanogr.* **132**, 250–261 (2015).
23. M. A. Spall, *J. Phys. Oceanogr.* **34**, 1197–1213 (2004).
24. F. Straneo, *J. Phys. Oceanogr.* **36**, 1822–1840 (2006).
25. R. S. Pickart, M. A. Spall, *J. Phys. Oceanogr.* **37**, 2207–2227 (2007).
26. G. D. McCarthy *et al.*, *Prog. Oceanogr.* **130**, 91–111 (2015).
27. G. Danabasoglu *et al.*, *Ocean Model.* **73**, 76–107 (2014).
28. J. Holte, F. Straneo, *J. Phys. Oceanogr.* **47**, 2531–2543 (2017).
29. A. Sarafanov *et al.*, *J. Geophys. Res. Oceans* **117**, C01014 (2012).
30. T. Rossby, G. Reverdin, L. Chafik, H. Søiland, *J. Geophys. Res. Oceans* **122**, 5870–5887 (2017).
31. K. E. Trenberth, J. M. Caron, *J. Clim.* **14**, 3433–3443 (2001).
32. R. Zantopp, J. Fischer, M. Visbeck, J. Karstensen, *J. Geophys. Res. Oceans* **122**, 1724–1748 (2017).
33. S. Zou, M. S. Lozier, *J. Phys. Oceanogr.* **46**, 2169–2182 (2016).
34. C. Eden, J. Willebrand, *J. Clim.* **14**, 2266–2280 (2001).
35. D. A. Bailey, P. B. Rhines, S. Häkkinen, *Clim. Dyn.* **25**, 497–516 (2005).
36. J. Getzlaff, C. W. Böning, C. Eden, A. Biastoch, *Geophys. Res. Lett.* **32**, L09602 (2005).
37. G. Danabasoglu *et al.*, *J. Clim.* **25**, 5153–5172 (2012).
38. J. Robson, P. Ortega, R. Sutton, *Nat. Geosci.* **9**, 513–517 (2016).
39. L. C. Jackson, K. A. Peterson, C. D. Roberts, R. A. Wood, *Nat. Geosci.* **9**, 518–522 (2016).
40. D. J. R. Thornalley *et al.*, *Nature* **556**, 227–230 (2018).
41. F. Li, M. S. Lozier, *J. Clim.* **31**, 5225–5241 (2018).
42. M. Bersch, I. Yashayaev, K. P. Koltermann, *Ocean Dyn.* **57**, 223–235 (2007).
43. K. Våge *et al.*, *Deep Sea Res. Part I Oceanogr. Res. Pap.* **58**, 590–614 (2011).
44. N. P. Holliday *et al.*, *J. Geophys. Res. Oceans* **120**, 5945–5967 (2015).
45. I. Yashayaev, J. W. Loder, *J. Geophys. Res. Oceans* **121**, 8095–8114 (2016).
46. Argo, Argo float data and metadata from Global Data Assembly Centre (Argo GDAC), SEANOE (2018); https://doi.org/10.17882/42182.
47. M. S. Lozier *et al.*, Meridional Overturning Circulation and the Associated Heat and Freshwater Transports Observed by the OSNAP Array from 2014 to 2016, Duke Digital Repository (2019); https://doi.org/10.7924/r4z60gf0f.
48. J. Karstensen, M. Oltmanns, OSNAP mooring data recovered during MSM54, PANGAEA (2018); https://doi.pangaea.de/10.1594/PANGAEA.896648.
49. Data Collection - OSNAP, Version OSNAP-V2-2018, Zenodo (2018); https://doi.org/10.5281/zenodo.1285757.
50. R. Pickart, Microcat, Aquadopp, ADCP, and Tidbit data from the 2014-2016 Labrador Sea eastern boundary mooring array as part of OSNAP, Duke Digital Repository (2018); https://doi.org/10.7924/r4fj2dr7k.
51. F. Straneo, A. Ramsey, F. Bahr, D. Torres, Microcat, current meter and ADCP data from the Cape Farewell mooring array southeast of Greenland as part of OSNAP, Duke Digital Repository (2018); https://doi.org/10.7924/r4fb50z9b.
52. N. P. Holliday, D. Rayner, S. Bacon, L. Houpert, Microcat, current meter and ADCP data from moorings of the Deep Western Boundary Current array (Irminger Sea) as part of UK OSNAP, British Oceanographic Data Centre - Natural Environment Research Council, UK (2018); https://doi.org/10/cwf4.
53. L. de Steur, M. F. de Jong, High-resolution current meter and hydrographic data from the Irminger Current mooring array 2014-2015, NIOZ Royal Netherlands Institute for Sea Research (2018); https://doi.org/10.4121/uuid:77b2c4fc-c253-4494-91bd-8d1ef66a014a.
54. L. de Steur, M. F. de Jong, High-resolution current meter and hydrographic data from the Irminger Current mooring array 2015-2016, NIOZ Royal Netherlands Institute for Sea Research (2018); https://doi.org/10.4121/uuid:9ae97ceb-39e4-43ec-abdb-614103285c16.
55. W. Johns, A. Houk, Microcat, current meter and ADCP data from the eastern mid-Atlantic ridge mooring array as part of OSNAP, Duke Digital Repository (2018); https://doi.org/10.7924/r42n52w5l.
56. J. Zhao, A. Bower, J. Yang, X. Lin, CTD data collected by Slocum glider operated between June and November 2015 in the Iceland Basin as part of OSNAP, Duke Digital Repository (2018); https://doi.org/10.7924/r4m905g03.
57. L. Houpert, M. E. Inall, E. Dumont, S. A. Cunningham, UK OSNAP near real-time glider dataset, British Oceanographic Data Centre - Natural Environment Research Council, UK (2018); https://doi.org/10/ckbr.
58. S. A. Cunningham, L. Houpert, E. Dumont, M. E. Inall, Microcat, current meter and ADCP data from moorings of the Eastern Boundary array (Rockall Trough) as part of UK OSNAP, British Oceanographic Data Centre - Natural Environment Research Council, UK (2018); https://doi.org/10/cwf3.

ACKNOWLEDGMENTS

We acknowledge fieldwork support provided by the officers, crews, and technicians of the R/V *Neil Armstrong*, R/V *Knorr*, R/V *Pelagia*, R/V *Maria S. Merian*, CCGS *Hudson*, and RRS *Discovery*. We thank E. Itsweire for his guidance and support during the initiation of this program. The Ssalto/Duacs altimeter products were produced and distributed by the Copernicus Marine and Environment Monitoring Service (CMEMS) (http://marine.copernicus.eu). **Funding:** We acknowledge funding from the Physical Oceanography Program of the U.S. National Science Foundation; the United Kingdom's Natural Environment Research Council programs UK-OSNAP, the Extended Ellett Line, and ACSIS (National Capability). Additional support was received from the European Union 7th Framework Programme (FP7 2007-2013) under grant 308299 (NACLIM) and the Horizon 2020 research and innovation program under grants 727852 (Blue-Action), 308299 (NACLIM), 678760 (ATLAS), and 633211 (AtlantOS). We

also acknowledge support from the French Centre National de la Recherche Scientifique and from China's national key research and development projects (2016YFA0601803) and the Fundamental Research Funds for the Central Universities (201424001). Support for the 53°N array by the RACE program of the German Ministry BMBF is acknowledged, as is the contribution from Fisheries and Oceans Canada's (DFO's) Atlantic Zone Off-shelf Monitoring Program (AZOMP). **Author contributions:** M.S.L., S.B., A.S.B., S.A.C., L.d.S., B.d.Y., J.F., B.J.W.G., N.P.H., M.E.I., W.E.J., H.L.J., J.K., X.L., D.P.M., R.S.P., F.S., V.T., R.G.W., and C.W. conceptualized and initiated the OSNAP project. M.S.L., S.B., A.S.B., S.A.C., L.d.S., B.d.Y., J.F., B.J.W.G., N.P.H., M.E.I., W.E.J., H.L.J., J.K., X.L., D.P.M., R.S.P., F.S., R.G.W., C.W., and J.Y. acquired financial support for the projects leading to this publication. M.S.L. managed and coordinated responsibilities for the research activity, planning, and execution. F.B., S.A.C., M.F.d.J., L.d.S., S.F.G., N.P.H., A.H., L.H., M.E.I., W.E.J., C.J., J.K., G.K., I.A.L.B., F.L., N.M., M.O., R.S.P., A.L.R., D.R., D.J.T., I.Y., and J.Z. were responsible for data collection, processing, and quality control. M.F.d.J., N.P.H., L.H., W.E.J., J.K., I.A.L.B., R.S.P., and J.Z. verified transport estimates at individual arrays. A.S.B., S.A.C., N.P.H., L.H., W.E.J., F.L., M.S.L., H.M., and C.W. developed data analysis methodology. F.L. synthesized the data and carried out data analyses. M.S.L. wrote the initial draft. F.L. prepared and created visualization/data presentation. S.B., A.S.B., S.A.C., M.F.d.J., L.d.S., B.d.Y., S.F.G., N.P.H., L.H., M.E.I., W.E.J., H.L.J., C.J., J.K., I.A.L.B., F.L., X.L., D.P.M., H.M., M.O., R.S.P., F.S., V.T., C.W., and R.G.W. reviewed and edited the manuscript. **Competing interests:** The authors declare that they have no competing interests. **Data and materials availability:** Argo data were collected and made freely available by the International Argo Program and the national programs that contribute to it (www.argo.ucsd.edu; http://argo.jcommops.org). The Argo Program is part of the Global Ocean Observing System (*46*). All data products from OSNAP, including those that support the main findings of this paper, are publicly available at www.o-snap.org. The derived data (i.e., MOC, MHT, and MFT) are also available in Duke Digital Repository (*47*). Calibrated and quality-controlled data from moored instruments and gliders were generated by each participating group: Canadian shelf break array (*48*), German 53°N array (*49*), U.S. Labrador Sea eastern boundary array (*50*), U.S. east Cape Farewell slope array (*51*), NOC DWBC array (*52*), NIOZ western Mid-Atlantic Ridge array (*53, 54*), U.S. eastern Mid-Atlantic Ridge array (*55*), WHOI/OUC gliders (*56*), SAMS gliders (*57*), and SAMS Rockall Trough array (*58*).

SUPPLEMENTARY MATERIALS

www.sciencemag.org/content/363/6426/516/suppl/DC1
Materials and Methods
Figs. S1 and S2
Tables S1 to S3
References (*59*–*72*)

5 July 2018; accepted 18 December 2018
10.1126/science.aau6592

A sea change in our view of overturning in the subpolar North Atlantic

M. S. Lozier, F. Li, S. Bacon, F. Bahr, A. S. Bower, S. A. Cunningham, M. F. de Jong, L. de Steur, B. deYoung, J. Fischer, S. F. Gary, B. J. W. Greenan, N. P. Holliday, A. Houk, L. Houpert, M. E. Inall, W. E. Johns, H. L. Johnson, C. Johnson, J. Karstensen, G. Koman, I. A. Le Bras, X. Lin, N. Mackay, D. P. Marshall, H. Mercier, M. Oltmanns, R. S. Pickart, A. L. Ramsey, D. Rayner, F. Straneo, V. Thierry, D. J. Torres, R. G. Williams, C. Wilson, J. Yang, I. Yashayaev and J. Zhao

Science **363** (6426), 516-521.
DOI: 10.1126/science.aau6592

An array of overturning data

The Atlantic meridional overturning circulation (AMOC) has a strong influence on climate, so it is important to understand how global warming may affect it. Lozier *et al.* report initial results from the Overturning in the Subpolar North Atlantic Program (OSNAP) (see the Perspective by Rhein). OSNAP has been measuring the flux of water transported by overturning in the high latitudes in the North Atlantic. The measurements reveal the strong variability of transport in the region and show that deep water formation in the Labrador Sea may not, as previously believed, be the major determinant of AMOC variability.

Science, this issue p. 516; see also p. 456